Surface & Coatings Technology 420 (2021) 127329

Contents lists available at ScienceDirect

Surface & Coatings Technology

journal homepage: www.elsevier.com/locate/surfcoat

Tribocorrosion-resistant biofunctionalized Ti-Al_2O_3 composites

L. Sousa [a,*], L. Basilio [a], A.C. Alves [a], F. Toptan [a,b,c]

[a] CMEMS-UMinho – Center of MicroElectroMechanical Systems – Universidade Minho, Campus de Azurém, Guimarães, Portugal
[b] IBTN/Euro – European Branch of the Institute of Biomaterials, Tribocorrosion and Nanomedicine, Dept. Eng. Mecânica, Universidade do Minho, Azurém, 4800-058 Guimarães, Portugal
[c] Department of Materials Science and Engineering, Izmir Institute of Technology, 35430, Urla, Izmir, Turkey

ARTICLE INFO

Keywords:
Titanium matrix composites
MAO
Corrosion
Tribocorrosion

ABSTRACT

Recent studies have shown that titanium matrix composites have potential for load-bearing biomedical implants due to their improved tribocorrosion behaviour compared to Ti and its alloys. However, lack of bioactivity remains as a concern due to bioinert Ti matrix and the fact that most reinforcement phases are also bioinert. In this work, biofunctionalized Ti-Al_2O_3 composites were produced by performing micro-arc oxidation treatment on the Ti-Al_2O_3 composites processed by hot-pressing technique. The overall microstructure consisted of Al_2O_3 particles dispersed within a biofunctionalized Ti matrix having a micro-porous structure rich in Ca and P elements. The corrosion behaviour of the composites was greatly improved after MAO treatment, whereas the tribocorrosion behaviour of the composites was also further improved after MAO treatment.

1. Introduction

Despite being widely used in hip-implants, Ti and its alloys still face some clinical concerns, such as low tribocorrosion resistance and lack of bioactivity. Regarding tribocorrosion resistance, it is well known that the addition of hard ceramic particles into a metal matrix can significantly improve the wear resistance of the metal matrix [1]. For that reason, titanium matrix composites (TMCs) have found several applications in the automotive and aerospace sectors and can also have potential in biomedical field, especially in load bearing orthopaedic implants. In the last few years some studies have reported that TMCs show a significant improvement on tribocorrosion behaviour compared to Ti, through reduced tendency to corrosion as well as reduced corrosion kinetics under a fretting or sliding action. Furthermore, a significant reduction in wear volume was also usually reported [2–4]. Among all the possible reinforcement phases, alumina (Al_2O_3), being a well know biomaterial, can be considered as an interesting choice to produce TMCs for biomedical applications. Alumina has been widely used in biomedical implants, being first used to replace the typical metallic femoral head of hip implants and today it is still used together with ultra-high molecular weight polyethylene which is a part of the acetabular component [5].

In total hip replacement, alumina-alumina bearings are known to be one of the most resistant to wear. Furthermore, low rate of osteolysis has also been reported due to exceptional wear resistance and low surface roughness of alumina [6–9]. Similar coefficient of thermal expansion (CTE) with Ti matrix and excellent compressive strength also make alumina a potential candidate for TMCs [10,11]. Ti-Al_2O_3 composites have shown good mechanical properties [12–14], overall good corrosion behaviour, even under acidic environments [15,16] and improved wear resistance [2], however tribocorrosion behaviour is still poorly understood.

Since most reinforcement phases are bioinert, the bioactivity of such composites continues to be an issue. While Ti-hydroxyapatite or Ti-bioactive glass composites have been reported to improve the bioactivity of Ti [17–20] their tribocorrosion behaviour is still poorly understood.

In order to improve the bioactivity, a range of surface modification techniques can be used, through thermal spraying, physical vapor deposition, chemical vapor deposition, coatings and anodic treatment (AT) [21,22]. AT is a promising technique since it can produce an oxide layer with tailored chemical and mechanical properties, as well with improved bioactivity and osteointegration capabilities [22–29]. Furthermore this technique has also been commercially used in dental implants [30]. Micro-arc oxidation (MAO) is a regime of AT, where several hundreds of voltage are used to produce a porous, crystalline,

* Corresponding author at: CMEMS-UMinho – Center of MicroElectroMechanical Systems – University of Minho – Department of Mechanical Engineering – Campus de Azurém, 4800-058 Guimarães, Portugal.
E-mail address: a65256@alunos.uminho.pt (L. Sousa).

https://doi.org/10.1016/j.surfcoat.2021.127329
Received 20 April 2021; Received in revised form 13 May 2021; Accepted 16 May 2021
Available online 24 May 2021

and thick TiO_2 layer that is recognized to improve the bioactivity of Ti [22–26]. Depending on the electrolyte composition, it is possible to incorporate bioactive elements on this layers, such as Ca and/or P. As an example, an electrolyte consisting of mixture of calcium acetate and beta-glycerophosphate disodium salt pentahydrate can be used to incorporate Ca and P and, depending on the processing conditions, Ca/P ratio can be controled [27,31]. In addition to the improved bioactivity, MAO layers also present other advantages that are of extreme importance for biomedical devices, such as reduced stiffness mismatches and additional corrosion and tribocorrosion resistance [32]. Ti-Al_2O_3 composites with a biofuncationalized titanium matrix could have potential to improve both the tribocorrosion and bioactivity of Ti. While the advantages of MAO treatment on Ti and Ti alloys have been widely reported in the last years, its effect on TMC surfaces is unknown, not only from a structure standpoint, but also its effects on the corrosion and tribocorrosion behaviour. One of the most critical aspects of TMCs resides in the interface between the Ti matrix and the reinforcement phases, as these interfaces will play an important role on the final properties of the composite, not only on the mechanical properties but also on the overall corrosion and tribocorrosion behaviour. Studies have shown that TiAl and Ti_3Al intermetallic phases form between Ti and Al_2O_3 due to their reaction during processing [2,12,15,16]. Additionally, the extension of this reaction will depend on the processing parameters such as processing temperature. Thus the objective of this work was to introduce biofunctionalized (MAO-treated) Ti-Al_2O_3 composites processed at two distinct temperatures as an alternative material for load-bearing implants and to study its corrosion and tribocorrosion behaviour.

2. Materials and methods

2.1. Processing

Ti matrix composites reinforced with 5% vol. of Al_2O_3 particles were processed by powder metallurgy. Both Ti grade 2 and 99.8% purity Al_2O_3 powders had irregular shapes (Fig. 1) with the particle size distribution presented on Table 1. Ball milling was used to mix the powders for 4 h at 120 rpm with the help of Al_2O_3 balls (ø 10 mm), under Ar atmosphere. Powder blends were placed in a zirconia coated graphite mould (10 mm inner diameter) in order to process samples with 3 mm of thickness. Hot-pressing was then carried out at high vacuum ($\leq 10^{-5}$ mbar) during 30 min under an applied pressure of 40 MPa. Two different sintering temperatures were used, namely 1000 °C and 1100 °C, 1100 °C was chosen based on a previous work [2], while 1000 °C was chosen in order to reduce the degree of reaction between the Al_2O_3 particles and the Ti matrix and observe its effect on the corrosion and tribocorrosion behaviour of these composites.

Table 1
Particle size distribution for Ti and Al_2O_3 powders.

	D[v,0.1] (μm)	D[v,0.5] (μm)	D[v,0.9] (μm)
Ti	10	25	44
Al_2O_3	17	42	71

Unreinforced Ti samples were also processed under identical conditions and used as control group. Depending on the sintering temperature, samples groups are referred as Ti_1000C and Ti-5Al_2O_3_1000C, Ti_1100C and Ti-5Al_2O_3_1100C. Before characterization and testing all samples were grinded down to 2400 mesh SiC papers and then mirror finished until 0.04 μm with colloidal silica suspension. Samples were then cleaned by propanol and distilled water in an ultrasonic bath for 10 and 5 min, respectively, and kept in a desiccator for 24 h prior to each test to obtain similar surface conditions.

2.2. Biofunctionalization

Biofunctionalization was conducted in an electrochemical cell connected to a DC power supply (Agilent technologies N5772A), as shown in detail in Fig. 2. MAO treatment was performed under a turbulent regime by means of a magnetic stirrer spinning at 200 rpm. A constant voltage of 300 V was applied for 1 min with an imposed current limit of 2.5 A. A mixture of 0.35 M of calcium acetate monohydrate (CA, Sigma-Aldrich) and 0.02 M of β-glycerophosphate disodium salt pentahydrate (β-GP, Alfa Aesar) was used as electrolyte. Hereafter, '_MAO' was added to the previous nomenclature in order to identify the biofunctionalized samples.

2.3. Electrochemical tests

The electrochemical behaviour was evaluated at body temperature (37 ± 2 °C) in phosphate-buffered saline (PBS) solution (0.24 g/L KH_2PO_4, 0.2 g/L KCl, 1.44 g/L Na_2HPO_4 8 g/L NaCl) having a pH adjusted to 7.4. Open circuit potential (OCP) was monitored until stabilization ($\Delta E < 60$ mV/h), followed by electrochemical impedance spectroscopy (EIS) measurements, which were scanned with a rate of 7 points per decade starting at 10^5 Hz until 10^{-2} Hz with an amplitude of the sinusoidal signal set at 10 mV. Finally, potentiodynamic polarization tests were performed by scanning at 1 mV/s a potential range from −0.2 V_{ocp} to 1.5 $V_{Ag/AgCl}$. For all electrochemical tests, a standard three-electrode setup was used consisting in a saturated Ag/AgCl reference electrode, a platinum (Pt) wire as counter electrode and the sample as working electrode. All the electrodes were connected to a Gamry

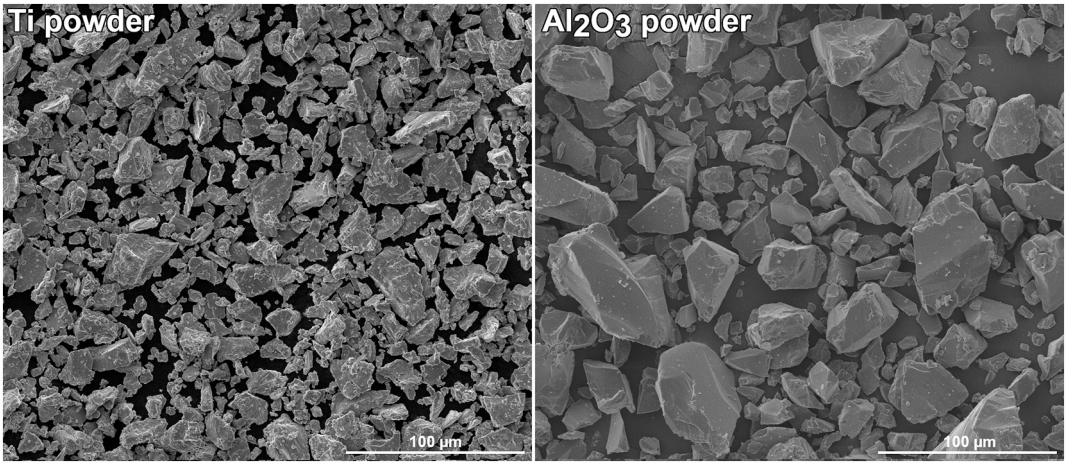

Fig. 1. SE SEM images of the raw Ti and Al_2O_3 powders.

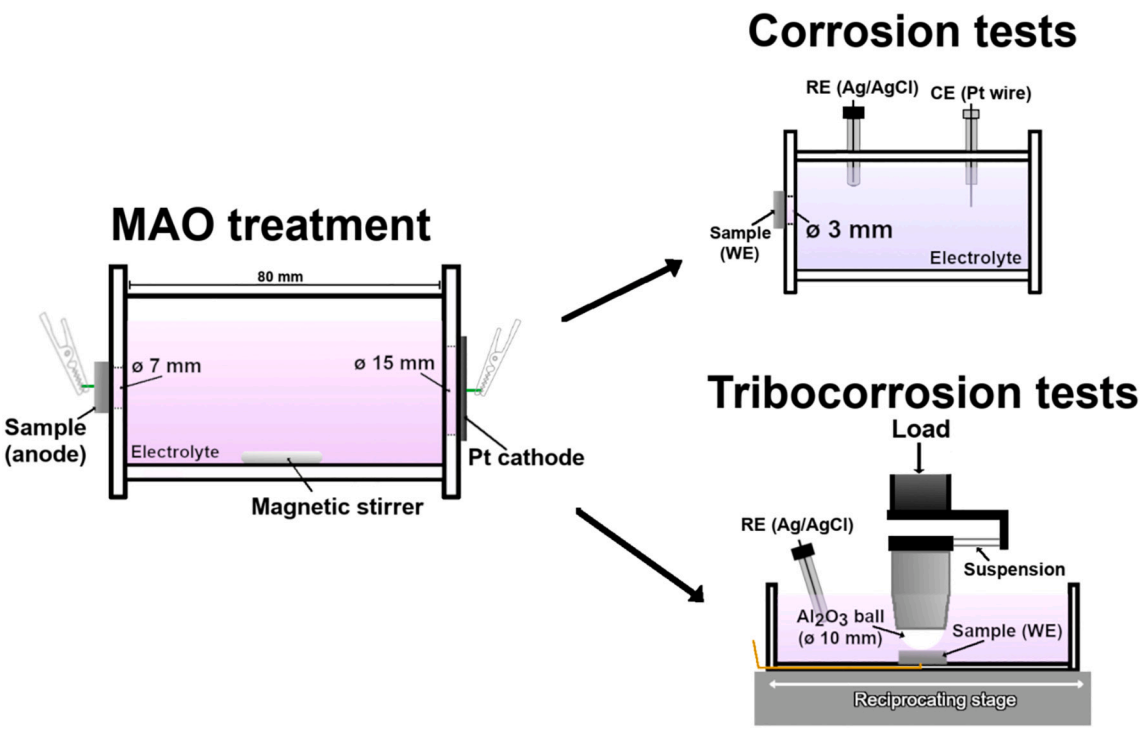

Fig. 2. General setup used in MAO treatments, together with corrosion and tribocorrosion tests.

Potentiostat/Galvanostat/ZRA (model Referece-600+). The general setup is described in Fig. 2.

2.4. Tribocorrosion tests

Tribocorrosion tests were performed in an identical PBS solution at body temperature. A tribo-electrochemical cell, placed in a tribometer (CETR-UMT2) with a ball-on-plate configuration and reciprocating stage, was used for all the tests, where an Al_2O_3 ball (ø 10 mm) slid against the untreated and MAO treated samples, as described in detail in Fig. 2. The OCP values were monitored before sliding until stabilization ($\Delta E < 60$ mV/h), under sling and after sliding for 1800 s. Coefficient of friction (COF) values were also monitored during sliding. The sliding action was performed under a 1 N of applied normal load (corresponds to a maximum Hertzian contact pressure for CP Ti of 0.41 GPa) during 30 min with 1 Hz frequency and total stroke length of 3 mm. The electrochemical tests were performed using a Gamry Potentiostat/Galvanostat/ZRA (model Referece-600) with a two-electrode set-up, where the samples were connected as working electrode and saturated Ag/AgCl reference electrode.

2.5. Characterization

The microstructures were analysed by field emission gun scanning electron microscope (FEG-SEM, FEI Nova 200), and the chemical compositions by EDAX energy dispersive X-ray spectroscopy (EDS). The crystalline structures of the MAO layers were evaluated by X-ray diffraction (Bruker D8 Discover diffractometer) at 40 kV with Cu Kα radiation. The overall hardness of the untreated samples was evaluated trough Vickers macro-hardness tests performed using an Officine Galileo Mod. D200 tester by applying 30 kgf load during 15 s by a mean of 5 indentations per sample, using 3 samples per condition. After tribocorrosion tests, samples were cleaned with the same cleaning procedure used on the metallographic preparation. The microstructures of the worn surfaces were then evaluated parallel to the sliding direction with the same FEG-SEM equipment and the wear track profiles were obtained by profilometry (Veeco, Dektak 150).

3. Results

3.1. Characterization

The overall microstructure of the as-processed composites, MAO treated Ti and MAO treated composites can be seen in the back scattered electron (BSE) and secondary electron (SE) SEM images presented in Fig. 3. Both Ti-Al_2O_3 composites presented a uniform distribution of reinforcement phases, with no signs of agglomerations. As it can be seen on the higher magnification images, a reaction zone between the Al_2O_3 particles and the Ti matrix was formed due to reaction between Ti and Al_2O_3. Comparing both processing temperatures, thicker reaction zones were obtained on Ti-Al_2O_3_1100C composites. On average, the thickness of the reaction zones was measured as 6 ± 1 and 11 ± 3 μm for composites processed at 1000 and 1100 °C, respectively.

Further inspection revealed that in both groups the reaction zone was formed by two distinct phases, marked in the figures as Z1 and Z2, where Z1 was much more predominant on composites processed at 1100 °C. The area ratio between the reaction zone and the Al_2O_3 particle increased with the increasing processing temperature, 1.16 and 2.95 for Ti-Al_2O_3_1000C and Ti-Al_2O_3_1100C, respectively.

EDS analysis showed that in both groups, Z1 and Z2 were constituted by a mixture of Ti and Al, with Z1 presenting Ti/Al at.% ratios close to 1 and Z2 showing Ti/Al ratios close to 3. The reaction products of Ti + Al_2O_3 belong to the Ti-Al-O system, where compounds such as Ti_3Al, TiAl, $TiAl_2$ and $TiAl_3$ and titanium oxides such as TiO and TiO_2 can be formed at the interface [33]. However due to limited diffusion capability of oxygen and high instability of $TiAl_2$ and $TiAl_3$ compounds at high temperatures [33], the reaction products are almost always TiAl and Ti_3Al [11,34,35], where the reaction sequence at 1100 °C is Al_2O_3/TiAl/Ti_3Al/Ti [11,34]. The results obtained were highly in accordance with the literature since Z1 corresponded to TiAl (Ti/Al ratio ≈ 1) and Z2 corresponded to Ti_3Al (Ti/Al ratio ≈ 3). It has also been reported that Ti_3Al is the first to be formed and, after Al enrichment, the formation of TiAl occurs. With low residence time and/or low temperature, the formation of TiAl can be reduced or avoided [33,36], that was probably the case on Ti-Al_2O_3_1000C composites, where the reaction zones tended to

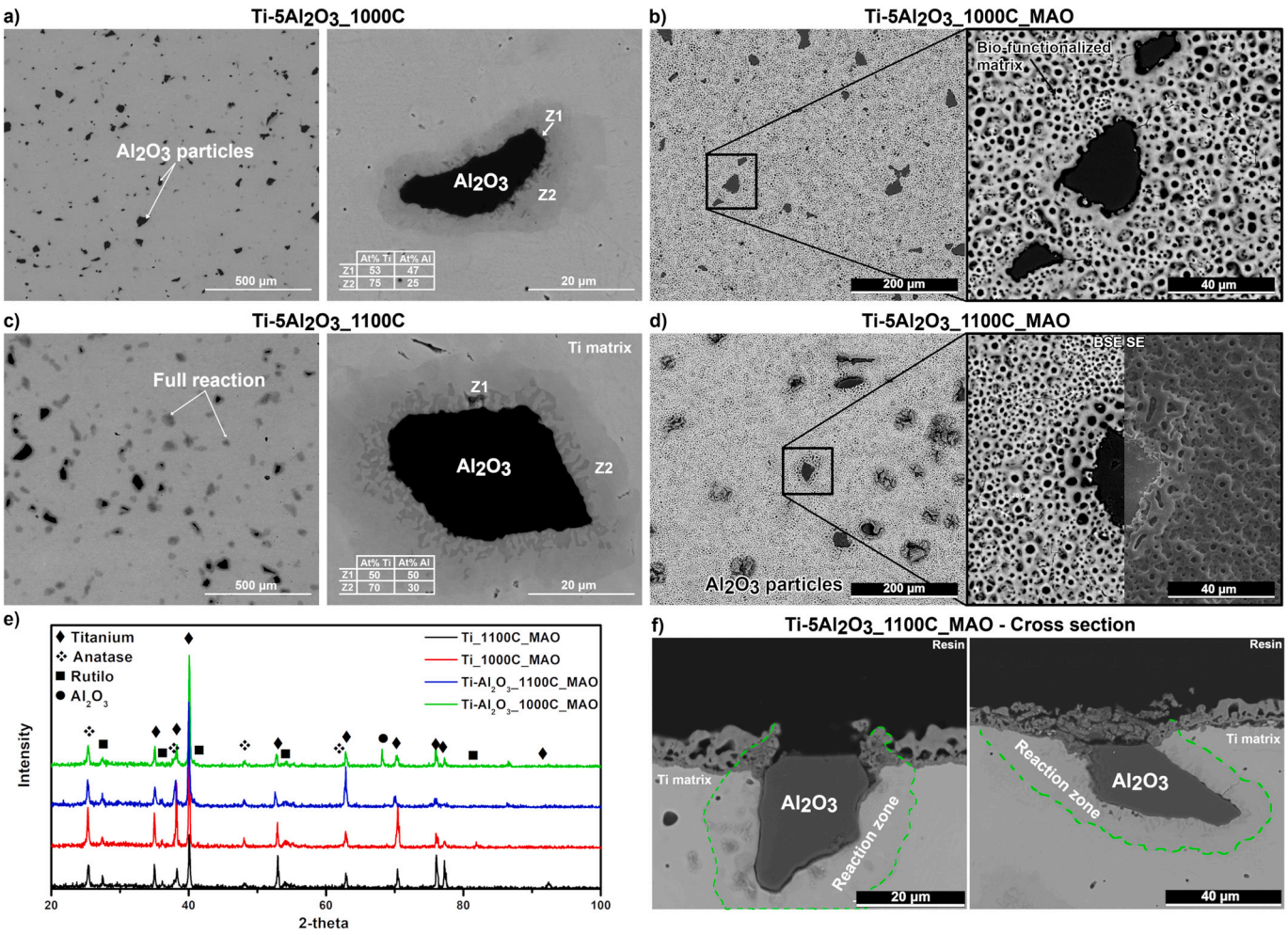

Fig. 3. Overall microstructure of the as-processed and biofunctionalized composites, Cross section BSE images from Ti-Al_2O_3_1100C group and XRD spectra for MAO treated groups.

be smaller and Z1 was much less predominant. Regarding the MAO treated groups, the typical volcano-like structure, usually reported in literature [31,37-39], was obtained for both unreinforced Ti groups, with no discernible differences between them. Ca/P at.% ratios were calculated as 3.02 ± 0.05 and 3.15 ± 0.12 for Ti_1000C_MAO and Ti_1100C_MAO respectively. XRD spectra, Fig. 3e, revealed a similar crystalline structure consisting of Ti and TiO_2 in the form of anatase and rutile phases.

For composite groups, MAO treatment led to the formation of the typical volcano-like structure. However, the MAO layer formed on the reaction zone seems to have some differences when compared with the one formed on Ti matrix, namely on the pores size and structure (Fig. 3d and f).

In addition, the cross sections also revealed on Ti matrix the usual MAO layer structure composed of a thin compact film next to the substrate followed by an inner and an outer porous layer [31]. However, the MAO layer formed on the reaction zone seems to be more heterogeneous and it is not possible to distinguish the two porous layers. XRD spectra presented in Fig. 3e, revealed the same crystalline structure obtained for Ti, being a mixture of anatase and rutile phases, with no discernible differences between all of the groups. Ca/P at.% ratio for composite groups were calculated as 2.96 ± 0.28 and 3.01 ± 0.07 for Ti-$5Al_2O_3$_1000C_MAO and Ti-$5Al_2O_3$_1100C_MAO, respectively, which were also in the same value ranges as the ones obtained for Ti groups.

3.2. Corrosion

Representative potentiodynamic polarization curves for untreated and biofunctionalized groups can be seen on Fig. 4. The average values obtained for OCP (E_{ocp}), corrosion potential ($E_{(i=0)}$) and passive current density (i_{pass}) can be seen on Table 2. For untreated samples, all the groups presented a well-defined passivation plateau, starting around 0.25 $V_{Ag/AgCl}$ for groups processed at 1000 °C and around 0.50 $V_{Ag/AgCl}$ for groups processed at 1100 °C. Ti and composites processed at 1100 °C presented slightly lower i_{pass} and higher E_{ocp} values while $E_{(i=0)}$ values were very similar to groups processed at 1000 °C. Comparing the general corrosion behaviour of untreated groups, it was observed that Ti-Al_2O_3_1100C group presented a distinct behaviour, where an abrupt increase in corrosion current density values was observed at 1.07 ± 0.19 as $V_{Ag/AgCl}$. Reinforcement phases may improve the corrosion behaviour of the base material by acting as inert physical barrier to corrosion [3] or by grain refinement of the metal matrix which may increase the quality of the native oxide film [40]. On the other hand, these reinforcement phases may also jeopardize the corrosion behaviour. Galvanic coupling between different phases including the metal matrix, reinforcement particles and/or phases formed at the reaction zones may lead to dissolution of the metal matrix and/or the reinforcement phases. [41]. On the other hand, the presence of porosity or defects at the interface between reinforcement/reaction zones/matrix interfaces may also lead to decreased corrosion resistance by leading to the formation of heterogeneities on the native oxide film [42,43]. Recent studies by

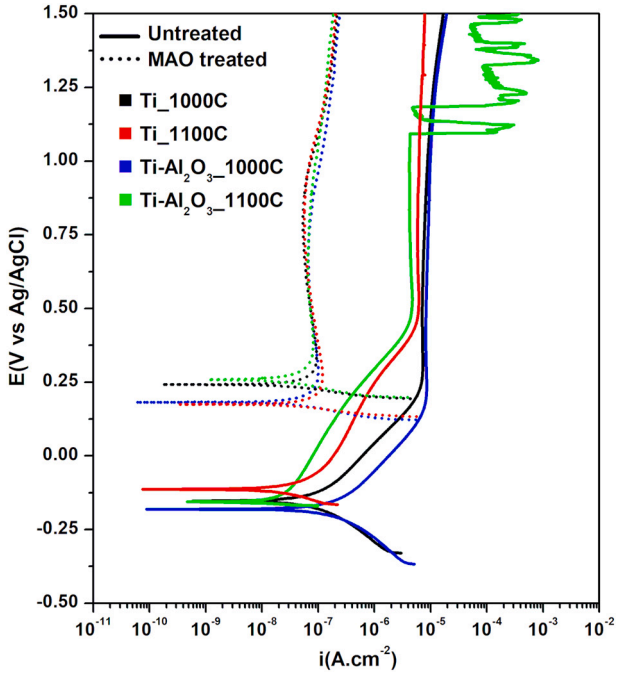

Fig. 4. Potentiodynamic polarization curves for all the conditions.

Table 2
E_{corr}, $E_{(i=0)}$ and i_{pass} values for all tested groups.

Group	E_{corr} (V)	$E_{(i=0)}$ (V)	i_{pass} (μAcm^2)
Ti_1000C	−0.14 ± 0.01	−0.15 ± 0.02	8.35 ± 0.70
Ti_1000C_MAO	0.39 ± 0.01	0.24 ± 0.01	0.06 ± 0.01
Ti-Al_2O_3_1000C	−0.15 ± 0.04	−0.16 ± 0.01	9.64 ± 1.36
Ti-Al_2O_3_1000C_MAO	0.33 ± 0.04	0.19 ± 0.04	0.07 ± 0.01
Ti_1100C	−0.03 ± 0.01	−0.12 ± 0.01	6.24 ± 1.30
Ti_1100C_MAO	0.27 ± 0.10	0.11 ± 0.10	0.07 ± 0.03
Ti-Al_2O_3_1100C	0.02 ± 0.01	−0.16 ± 0.03	4.63 ± 0.40
Ti-Al_2O_3_1100C_MAO	0.36 ± 0.03	0.21 ± 0.05	0.07 ± 0.01

Bahraminasab et al. [15,16] showed that adding Al_2O_3 particles into a Ti matrix, may have a dual effect on the corrosion behaviour of the composites. On one hand the presence of Al_2O_3 particles lead to an improvement of the overall corrosion resistance when compared with unreinforced Ti, due to the formation of a higher quality native oxide film, however for higher percentages of reinforcement phases, the authors reported that the corrosion behaviour was lower than unreinforced Ti, probably due to higher percentages of TiAl and Ti_3Al brittle phases which may have increased susceptibility to corrosion. Rocha et al. [34] showed that the corrosion behaviour of Ti/Al_2O_3 interfaces was heavily influenced by the presence of TiAl intermetallic phase, as this phase was found to be corrosion susceptible. Accordingly, the corrosion behaviour obtained for Ti-Al_2O_3_1100C group may be explained by the presence of more interfacial zones.

After MAO treatment all the groups presented a considerable increase in corrosion resistance as can be seen by the almost 2 decades decrease in i_{pass} values. The corrosion behaviour is characterized by a well-defined passivation plateau, where the current density values have a range of variation of about half a decade. A similar increase in corrosion resistance on MAO treated Ti has previously been reported [39,44].

The improvement on the corrosion behaviour is associated to the formation of a triplex layer, having a dense barrier layer between the Ti substrate and the outer porous layers with improved corrosion resistance [31,39]. By analysing the potentiodynamic polarization curves and the values presented on Table 2, no discernible differences between the MAO treated groups were observed. The presence of Al_2O_3 particles and adjacent reaction zones in the Ti matrix did not jeopardize the good corrosion behaviour of these layers, additionally the possible adverse effect of the reaction zones observed on Ti-Al_2O_3_1100C group was completely avoided, as the Ti-Al_2O_3_1100C_MAO group presented similar behaviour to the other MAO groups. In addition, the heterogonies observed on the MAO layer for this groups did not affect the overall corrosion behaviour.

3.3. Tribocorrosion behaviour

Fig. 5 shows the evolution of OCP before, during and after sliding action, as well as the evolution of COF values during sliding for all the groups. Before sliding, all the untreated groups presented stable OCP values due to formation of a stable native oxide film. Immediately after sliding started, all the groups presented a sharp decrease in OCP values due to the mechanical damage given to the native oxide film and consequence exposure of fresh metallic areas to the electrolyte. For Ti groups, OCP values dropped 670 ± 90 and 837 ± 50 mV for Ti_1100C and Ti_1000C respectively, while composite groups presented OCP drops of 490 ± 17 and 527 ± 81 mV for Ti-Al_2O_3_1100C and Ti-Al_2O_3_1000C respectively. Overall, no significant differences were observed on OCP evolution between both Ti and composites groups.

During sliding, large fluctuations on OCP and respective COF values were observed for all the untreated groups. This behaviour can be attributed to the continuous formation and breaking of discontinuous tribolayers, which can be seen on BSE SEM images shown in Fig. 6. These tribolayers, which were formed due to compaction of wear debris on the wear track, gave limited protection against corrosion, as they protected the metallic area to some extent, and consequently an increase in OCP values was observed. When these tribolayers reached a critical thickness and broke, fresh metallic areas were exposed to the electrolyte and a consequent decrease in OCP values was observed. This behaviour was also reflected on the COF values, where an increase in OCP is accompanied by an increase in COF, which is related with the increase in surface roughness due to formation of these tribolayers. Overall, COF values were lower for both composite groups, which can be attributed to the low COF alumina-alumina tribological contacts happening to some extent on the wear track, as well as the less formation of tribolayers, due to less metallic area being available for material pull-out and also due to overall higher hardness of the composite surfaces. Immediately after sliding, OCP values rapidly recovered to the ones observed before sliding due to repassivation of the worn zones.

All the MAO treated groups presented a substantial improvement on the tribocorrosion behaviour. Before sliding, these groups presented considerably lower tendency to corrosion due to the protective nature of the MAO layers. During the entire time of sliding, no noticeable drops in OCP values were observed, suggesting that not enough mechanical damage was given to reach the bulk material. SE and BSE SEM images of the worn surfaces are given in Fig. 7 showing the typical volcano-like structure on the worn areas. The high wear resistance of MAO layers has been attributed to the high hardness of anatase and rutile phases, where rutile is probably more effective since it possesses higher hardness than anatase [37]. COF evolution was very similar for all MAO treated groups, characterized by a run-in period in the initial 200–600 s, and then a slowly increase in COF values were observed until the end of sliding.

Fig. 6 shows representative BSE SE SEM images of the worn surfaces for untreated groups. Both Ti groups presented similar morphology, where the worn surfaces were composed of discontinuous tribolayers and parallel grooves to the sliding direction. During sliding, a considerable amount of metal may be pulled out from the wear track by the counter-body due to adhesive wear, as confirmed by the chemical analysis performed on the counter-body surfaces (Fig. 6). Consequently, this adhered material can transfer repetitively between the sliding surfaces and may be compacted on the wear track, leading to the formation

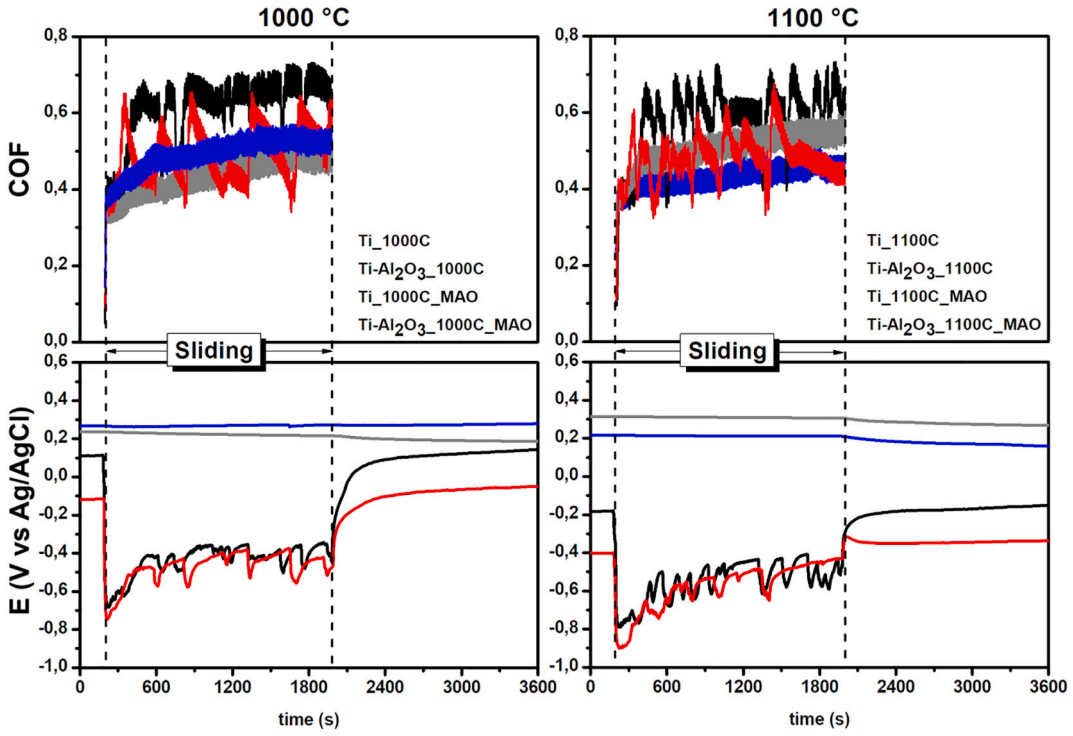

Fig. 5. Evolution of OCP before, during and after sliding, together with the respective COF values registered during sliding.

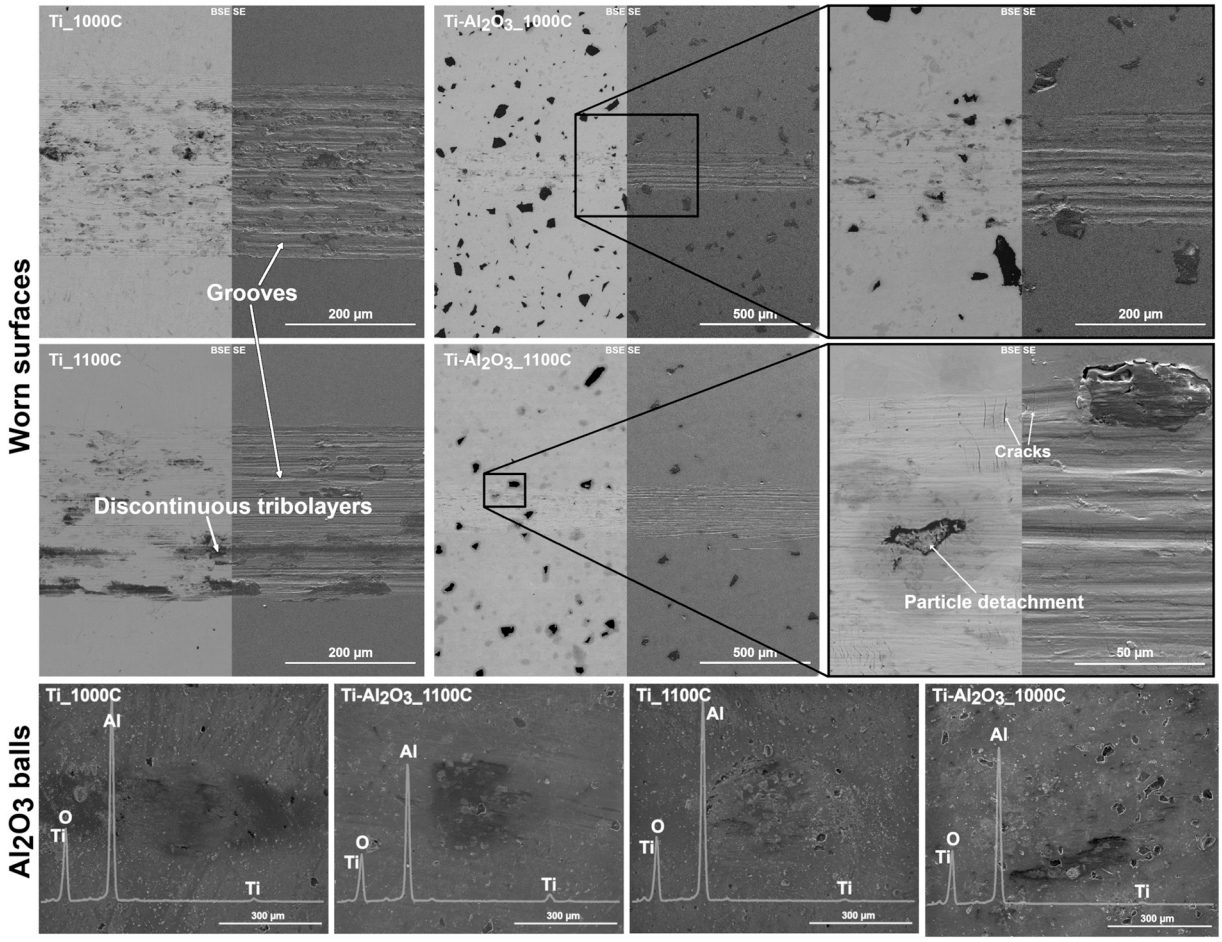

Fig. 6. BSE and SE SEM images of the worn surfaces for untreated groups after tribocorrosion tests together with SE SEM images of the Al_2O_3 balls used as counter-body and respective overall chemical composition of these surfaces.

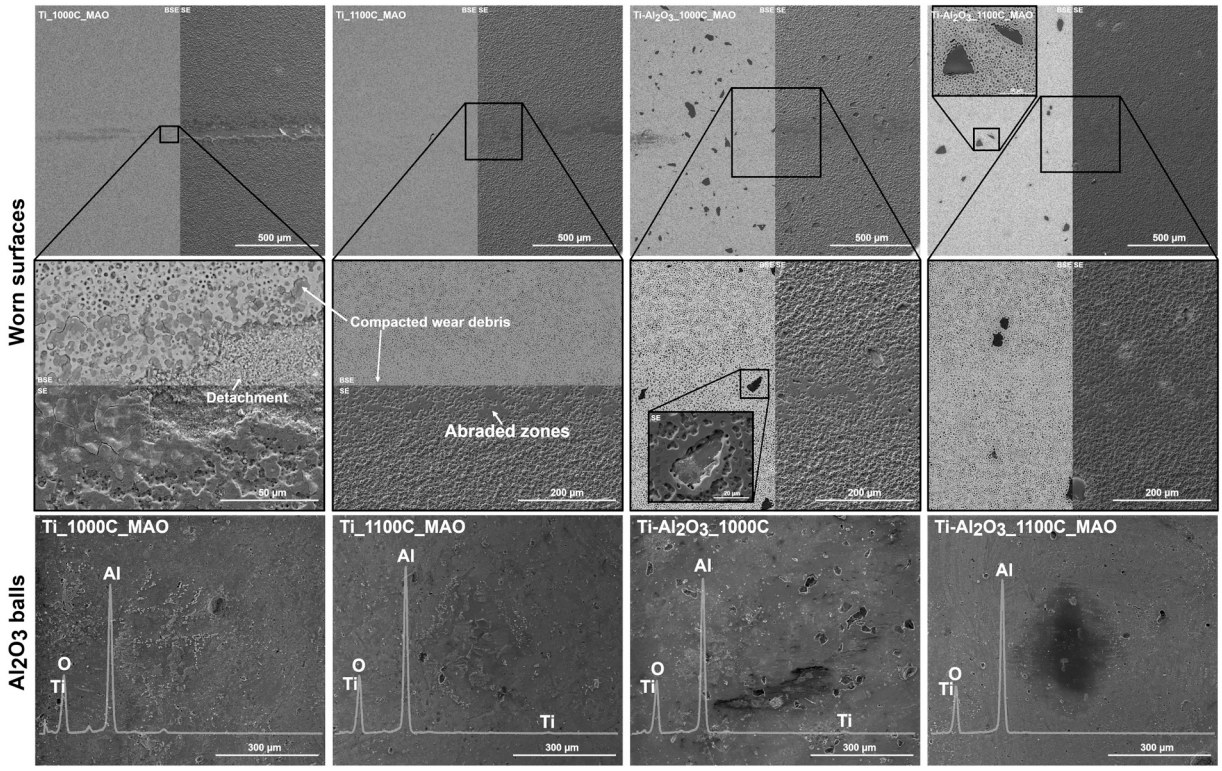

Fig. 7. BSE and SE SEM images of the worn surfaces for MAO treated groups after tribocorrosion tests.

of tribolayers, adhered to the counter-body and/or move freely on the wear track. Due to repetitive transfer of material, this adhered material tends to get harder and act as an abrasive, leading to the formation of grooves on the worn surfaces. Besides, non-adhered, freely moving wear debris can act as an extra abrasive. Composite groups also presented similar features, where discontinuous tribolayers and grooves were observed on the wear tracks. Additionally, it was observed that Ti-Al_2O_3_1100C group presented some Al_2O_3 particle detachments and small cracks perpendicular to the sliding direction, whereas these features were not observed on Ti-Al_2O_3_1000C group. Fig. 8 shows optical microscope images of representative Vickers indentation for each composite group. As can be seen, the indentations performed on Ti-Al_2O_3_1100C group lead to the formation of cracks at the corners of the indentation, which are in accordance with a Palmqvist crack system, also reported by other authors on Ti-Al_2O_3 systems [12]. The length of these cracks may be used to estimate fracture toughness (*Kc*) by the means of Eq. (1), where H_v is Vickers hardness, *a* is half of the diagonal of the Vickers indentation, *l* is the length of the crack starting from the corner of the indentation and *E* is the Young's modulus. The *E* values used in the calculations were estimated by rule of mixtures by taking in consideration reported Young's modulus from CP Ti 2 and Al_2O_3 (around 120 GPa and 380 GPa, respectively [12]).

$$K_C = 0.0264(H_v a)\left(\frac{E}{H_V}\right)^{0.4}\left(l^{-0.5}\right) \quad (1)$$

The *Kc* values for Ti-Al_2O_3_1100C group were estimated as 6.6 ± 0.4

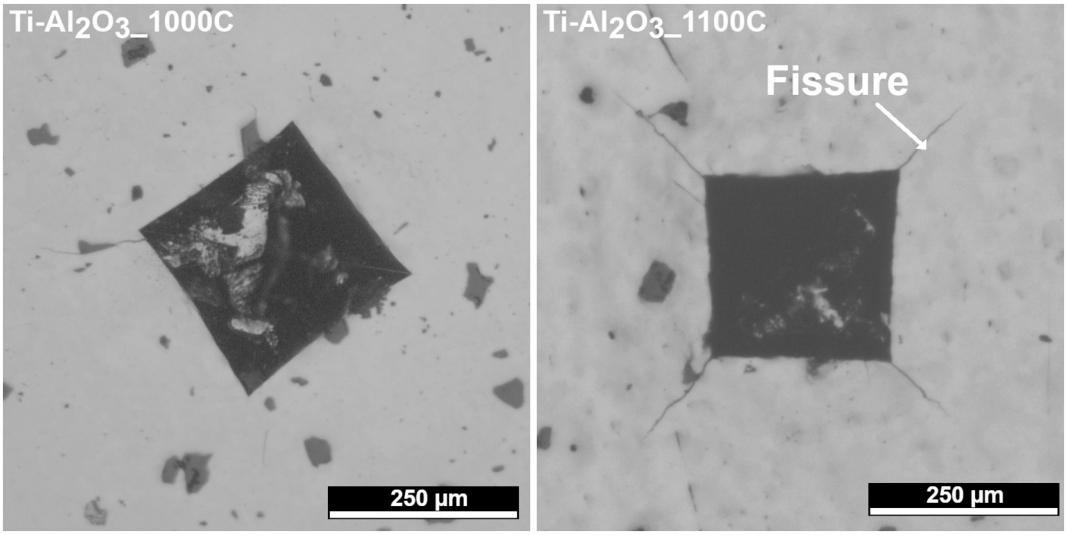

Fig. 8. Representative optical microscope (OM) images of Vickers indentations for each composite group.

MPa·m$^{0.5}$, which are considerably lower than the ones usually observed for CP Ti grade 2 (≈60 MPa·m$^{0.5}$ [45]). Since these cracks were not present on Ti-Al_2O_3_1000C group, it was not possible to estimate *Kc* values by this method. However, it is reasonable to assume that this group presented higher fracture toughness by the fact that these cracks around the indentations were not observed. Bahraminasab et al. [14] reported that the low fracture toughness of Ti-Al_2O_3 composites was often associated with the formation of Ti_3Al and TiAl intermetallic phases, characterized by their brittle nature. In addition, these phases may also lead to Al_2O_3 particle pull-out due to low strength ceramic/matrix interface. The morphology observed on the wear tracks for Ti-Al_2O_3_1100C group are most probably related to these factors. Due to higher processing temperature, a higher amount of TiAl and Ti_3Al intermetallic were obtained, due to higher area of reaction zones. During sliding, even relatively lower contact pressures may induce the formation and propagation of cracks. If these cracks are propagated trough the intermetallic phases surrounding the Al_2O_3 particles, particle pull-out may occur. Thus, due to lower amount of such intermetallic phases on Ti-Al_2O_3_1000C group and consequently higher fracture toughness, no visible cracks were formed during sliding, at least under these conditions.

The worn surfaces of MAO treated groups can be seen on Fig. 7. Under these conditions, no significant wear was observed for any of the treated groups, hence, BSE images showing no evidence of considerable metallic area being exposed to the electrolyte. The worn surfaces presented a smoother appearance once the outer pores were compacted/abraded by the counter-body. Additionally, the adjacent pores on the lower topographic planes served as wear debris reservoirs, where wear debris compacted inside the pores could be seen. Important to note that for Ti_1000C_MAO group, some detachments of the outer porous layer were observed, where the volcano-like structure was lost. Nevertheless, chemical analysis in these zones still showed considerable amount of Ca and P elements, although the Ca/P ratio decreased to about 0.99. SE SEM images and chemical analysis of the counter-body surfaces are also presented in Fig. 7. Very small amounts of Ti were found on the counter-body surfaces, probably due to some material transfer from the TiO_2 MAO layer during sliding action.

No considerable differences were observed between the MAO treated composites. As can be seen on the SE SEM images given in Fig. 7, the majority of Al_2O_3 particles were in lower topographic planes than the outer porous layer and under these testing conditions, no significant wear damage was done on the MAO surfaces exposing the reinforcing particles to the counter-material. Thus, under these tribological testing conditions, on MAO treated composites, direct role of the reinforcing particles on wear resistance by the load-carrying effect was not significantly occurred. Instead, indirect effect of the particle incorporation probably improved the overall wear resistance by strengthening the matrix and increasing the hardness of the base material.

Representative wear track profiles together with the average wear volume values for untreated groups can be seen on Fig. 9. Since no significant wear was observed on the MAO treated groups, it was not possible to measure wear volume loss for these groups. Ti groups presented practically the same behaviour with no differences on the average wear volume loss values. Composites presented about 50% reduction in wear volume loss, with Ti-Al_2O_3_1000C group showing the lowest values, which is probably attributed to the increased fracture toughness compared to the other composite group.

The corrosion and tribocorrosion behaviour of Ti-Al_2O_3 composites were improved after MAO treatment, with an expected improvement on biological behaviour considering that the overall structure of the MAO layers, in terms of chemical/phase composition as well as morphology, were very similar to the ones already reported on Ti [46]. Even though, before considering these composites for load-bearing implants in contact with bone, the tribological consequences of the relative motions on bones against these composites should be investigated in depth. Afterwards, surface composition and topography should be optimized in order to obtain the optimum tribo-electrochemical and biological performance.

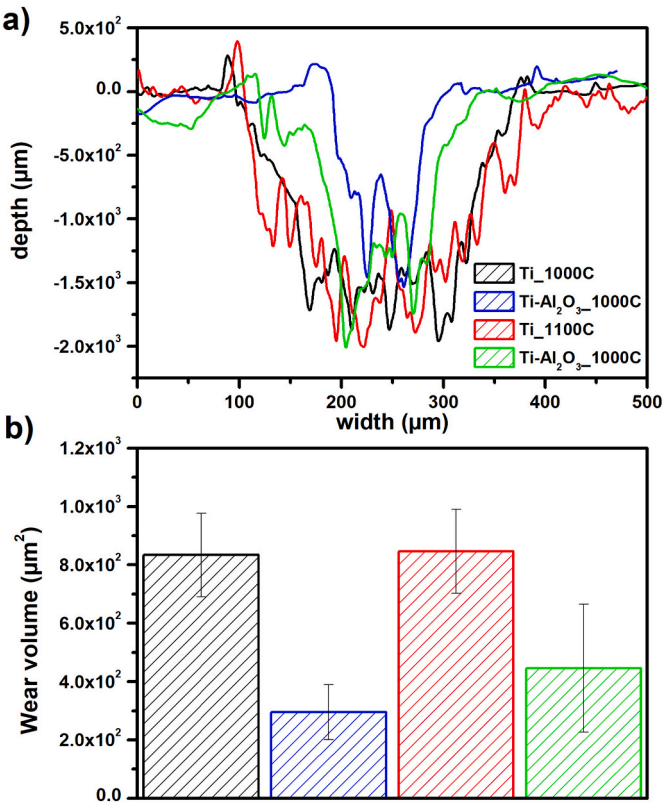

Fig. 9. (a) Representative wear track profiles and (b) average wear volume loss values calculated from wear profiles.

3.4. Conclusions

Ti-Al_2O_3 composites with a biofunctionalized Ti matrix were successfully produced by performing MAO treatment on Ti-Al_2O_3 composites. The extension of the reaction zone formed due to Ti and Al_2O_3 reaction influenced the corrosion and tribocorrosion behaviour of the as processed composites. In addition, these reaction zones lead to some heterogeneities in the structure of the MAO layer.

After MAO treatment, composites presented a significant improvement on the corrosion behaviour, and the possible negative effect of the reaction zone was avoided. Composites showed an improvement on tribocorrosion behaviour compared to unreinforced Ti through reduced overall wear volume losses. After MAO treatment the tribocorrosion behaviour was further improved.

Declaration of competing interest

The authors declare that they have no known competing financial interests or personal relationships that could have appeared to influence the work reported in this paper.

Acknowledgements

This work was supported by Portuguese FCT, under UIDB/04436/2020 and M-ERA-NET/0001/2015 projects. L. Sousa was grateful for the PhD grant through NORTE-08-5369-FSE-000051 project.

References

[1] N. Chawla, Y.L. Shen, Mechanical behavior of particle reinforced metal matrix composites, Adv. Eng. Mater. 3 (2001) 357–370.
[2] A. Oliveira, F. Toptan, Wear behavior of Ti-Al2O3 biocomposites in 9 g/L NaCl solution, J. Mater. Eng. Perform. 28 (2019) 6000–6010.
[3] J.I. Silva, A.C. Alves, A.M. Pinto, F. Toptan, Corrosion and tribocorrosion behavior of Ti−TiB−TiNx in-situ hybrid composite synthesized by reactive hot pressing, J. Mech. Behav. Biomed. Mater. 74 (2017) 195–203.
[4] F. Toptan, A. Rego, A.C. Alves, A. Guedes, Corrosion and tribocorrosion behavior of Ti–B4C composite intended for orthopaedic implants, J. Mech. Behav. Biomed. Mater. 61 (2016) 152–163.
[5] M. Navarro, A. Michiardi, O. Castaño, J.A. Planell, Biomaterials in orthopaedics, J. Chem. Technol. Biotechnol. (2008) 1137–1158.
[6] S. Affatato, F. Traina, M. De Fine, S. Carmignato, A. Toni, Alumina-on-alumina hip implants: a wear study of retrieved components, J. Bone Jt. Surg. - Br. 94–B (2012) 37–42.
[7] S. Affatato, F. Traina, A. Toni, Microseparation and stripe wear in alumina-on-alumina hip implants, Int. J. Artif. Organs 34 (2011) 506–512.
[8] P. Boyer, D. Huten, P. Loriaut, V. Lestrat, C. Jeanrot, P. Massin, Is alumina-on-alumina ceramic bearings total hip replacement the right choice in patients younger than 50 years of age? A 7 to 15 year follow-up study, Orthop. Traumatol. Surg. Res. 96 (2010) 616–622.
[9] B. Masson, Emergence of the alumina matrix composite in total hip arthroplasty, Int. Orthop. 33 (2009) 359–363.
[10] M. Liu, Z. Wang, J. Wu, Q. Li, Effects of Nd2O3 on the mechanical properties and oxidation behavior of Ti/Al2O3 composites by vacuum hot pressing sintering, J. Alloys Compd. 648 (2015) 116–121.
[11] G.P. Kelkar, A.H. Carim, Phase Equilibria in the Ti-Al-O system at 945 °C and analysis of Ti/Al2O3 reactions, J. Am. Ceram. Soc. 3 (1995) 572–573.
[12] S. Meir, S. Kalabukhov, N. Frage, S. Hayun, Mechanical properties of Al2O3\Ti composites fabricated by spark plasma sintering, Ceram. Int. 41 (2015) 4637–4643.
[13] T. Fujii, K. Tohgo, M. Iwao, Y. Shimamura, Fabrication of alumina-titanium composites by spark plasma sintering and their mechanical properties, J. Alloys Compd. 744 (2018) 759–768.
[14] M. Bahraminasab, S. Ghaffari, H. Eslami-Shahed, Al2O3-Ti functionally graded material prepared by spark plasma sintering for orthopaedic applications, J. Mech. Behav. Biomed. Mater. 72 (2017) 82–89.
[15] M. Bahraminasab, M. Bozorg, S. Ghaffari, F. Kavakebian, Electrochemical corrosion of Ti-Al2O3 biocomposites in Ringer's solution, J. Alloys Compd. 777 (2019) 34–43.
[16] M. Bahraminasab, M. Bozorg, S. Ghaffari, F. Kavakebian, Corrosion of Al2O3-Ti composites under inflammatory condition in simulated physiological solution, Mater. Sci. Eng. C. 102 (2019) 200–211.
[17] C.Q. Ning, Y. Zhou, In vitro bioactivity of a biocomposite fabricated from HA and Ti powders by powder metallurgy method 23 (2002) 2909–2915.
[18] H. Ye, X. Yang, H. Hong, Cladding of titanium/hydroxyapatite composites onto Ti6Al4V for load-bearing implant applications, Mater. Sci. Eng. C 29 (2009) 2036–2044.
[19] E. Verne, M. Ferraris, A. Ventrella, L. Paracchini, A. Krajewski, Sintering and Plasma Spray Deposition of Bioactive Glass-Matrix Composites for Medical Applications, J. Eur. Ceram. Soc. 18 (1998) 363–372.
[20] C. Ning, Y. Zhou, Correlations between the in vitro and in vivo bioactivity of the Ti/HA composites fabricated by a powder metallurgy method, Acta Biomater. 4 (2008) 1944–1952.
[21] Y. Wang, H. Yu, C. Chen, Z. Zhao, Review of the biocompatibility of micro-arc oxidation coated titanium alloys, Mater. Des. 85 (2015) 640–652.
[22] C. Chang, X. Huang, Y. Liu, L. Bai, X. Yang, R. Hang, B. Tang, P.K. Chu, High-current anodization: a novel strategy to functionalize titanium-based biomaterials, Electrochim. Acta 173 (2015) 345–353.
[23] Y. Zhao, T.-Y. Xiong, Formation of bioactive titania films under specific anodisation conditions, Surf. Eng. 28 (2012) 371–376.
[24] B. Yang, M. Uchida, H.M. Kim, X. Zhang, T. Kokubo, Preparation of bioactive titanium metal via anodic oxidation treatment, Biomaterials. 25 (2004) 1003–1010.
[25] Y. Li, B. Li, X. Fu, J. Li, C. Li, H. Li, H. Li, C. Liang, H. Wang, L. Zhou, S. Xin, Anodic oxidation modification improve bioactivity and biocompatibility of titanium implant surface, J. Hard Tissue Biol. 22 (2013) 351–358.
[26] M. Tsai, Y. Chang, H. Huang, Y. Wu, T. Shieh, Micro-arc oxidation treatment enhanced the biological performance of human osteosarcoma cell line and human skin fibroblasts cultured on titanium – zirconium films, Surf. Coat. Technol. 303 (2016) 268–276.
[27] G.G. Lima, G.B. Souza, C.M. Lepienski, N.K. Kuromoto, Mechanical properties of anodic titanium films containing ions of Ca and P submitted to heat and hydrothermal treatment, J. Mech. Behav. Biomed. Mater. 64 (2016) 18–30.
[28] N.F. Daudt, M. Bram, A.P. Cysne Barbosa, C. Alves, Surface modification of highly porous titanium by plasma treatment, Mater. Lett. 141 (2015) 194–197.
[29] C. Wang, Y. Bai, Y. Bai, J. Gao, W. Ma, Enhancement of corrosion resistance and bioactivity of titanium by Au nanoparticle-loaded TiO2 nanotube layer, Surf. Coat. Technol. 286 (2016) 327–334.
[30] A. Aalam, H. Nowzari, Clinical Evaluation of Dental Implants With Surfaces Roughened by Anodic Oxidation, Dual Acid-etched Implants, and Machined Implants, Int. J. Oral Maxillofac. Implants (2005) 793–798.
[31] A.C. Alves, F. Wenger, P. Ponthiaux, J.P. Celis, A.M. Pinto, L.A. Rocha, J.C. S. Fernandes, Corrosion mechanisms in titanium oxide-based films produced by anodic treatment, Electrochim. Acta 234 (2017) 16–27.
[32] G. Ryan, A. Pandit, D.P. Apatsidis, Fabrication methods of porous metals for use in orthopaedic applications, Biomaterials. 27 (2006) 2651–2670.
[33] M. Liu, Z. Wang, J. Wu, Q. Li, Ti/Al2O3 interfacial diffusion: kinetic equation for growth of reaction layer and formation mechanism, J. Alloys Compd. 652 (2015) 260–265.
[34] L.A. Rocha, E. Ariza, A.M. Costa, FJ. Oliveira, R.F. Silva, Electrochemical behavior of Ti/Al2O3 interfaces produced by diffusion bonding, Mater. Res. 6 (2003) 439–444.
[35] L.E. Karkina, L.I. Yakovenkova, Dislocation core structure and deformation behavior of Ti3Al, Mater. Sci. Eng. 20 (2012) 0–20.
[36] A.M. Kliauga, M. Ferrante, Interface compounds formed during the diffusion bonding of Al2O3 to Ti, J. Mater. Sci. 35 (2000) 4243–4249.
[37] A.C. Alves, F. Oliveira, F. Wenger, P. Ponthiaux, J.-P. Celis, L.A. Rocha, Tribocorrosion behaviour of anodic treated titanium surfaces intended for dental implants, J. Phys. D. Appl. Phys. 46 (2013), 404001.
[38] F. Witte, V. Kaese, H. Haferkamp, E. Switzer, A. Meyer-Lindenberg, C.J. Wirth, H. Windhagen, In vivo corrosion of four magnesium alloys and the associated bone response, Biomaterials. 26 (2005) 3557–3563.
[39] A.I. Costa, L. Sousa, A.C. Alves, F. Toptan, Tribocorrosion behaviour of bio-functionalized porous Ti surfaces obtained by two-step anodic treatment, Corros. Sci. 166 (2020), 108467.
[40] Y. Chen, J. Zhang, N. Dai, P. Qin, H. Attar, L.-C. Zhang, Corrosion behaviour of selective laser melted Ti-TiB biocomposite in simulated body fluid, Electrochim. Acta 232 (2017) 89–97.
[41] M. Rani, D. Kim, E. Fleury, Intermetallics dependency of the corrosion properties of in-situ Ti-based BMG matrix composites with the volume fraction of crystalline phase, Intermetallics. 22 (2012) 255–259.
[42] B. Bobić, S. Mitrović, M. Babić, I. Bobić, Corrosion of metal-matrix composites with aluminium alloy substrate, Tribol. Ind. 32 (2010) 3–11.
[43] S.C. Ferreira, L.A. Rocha, E. Ariza, P.D. Sequeira, Y. Watanabe, J.C.S. Fernandes, Corrosion behaviour of Al/Al3Ti and Al/Al3Zr functionally graded materials produced by centrifugal solid-particle method: influence of the intermetallics volume fraction, Corros. Sci. 53 (2011) 2058–2065.
[44] F.G. Oliveira, A.R. Ribeiro, G. Perez, B.S. Archanjo, C.P. Gouvea, J.R. Araújo, A.P. C. Campos, A. Kuznetsov, C.M. Almeida, M.M. Maru, C.A. Achete, P. Ponthiaux, J. P. Celis, L.A. Rocha, Understanding growth mechanisms and tribocorrosion behaviour of porous TiO2 anodic films containing calcium, phosphorous and magnesium, Appl. Surf. Sci. 341 (2015) 1–12.
[45] M. Niinomi, Mechanical properties of biomedical titanium alloys, Mater. Sci. Eng. A 243 (1998) 231–236.
[46] A.C. Alves, R. Thibeaux, F. Toptan, A.M.P. Pinto, P. Ponthiaux, B. David, Influence of macroporosity on NIH/3T3 adhesion, proliferation, and osteogenic differentiation of MC3T3-E1 over bio-functionalized highly porous titanium implant material, J. Biomed. Mater. Res. B Appl. Biomater. (2018) 1–13.